Research Square

Preprints are preliminary reports that have not undergone peer review.
They should not be considered conclusive, used to inform clinical practice,
or referenced by the media as validated information.

Experimental and numerical investigation of some impeller geometric parameters of an industrial electric submersible pump

Zeynel Abbidin Firatoglu (firatoglu@harran.edu.tr)
Harran Universitesi https://orcid.org/0000-0002-2791-6663
Mustafa Nuri Alihanoglu
Harran Universitesi

Original Article

Keywords: Submersible pump, CFD simulations, experimental measurements, flow structure, geometric parameters

Posted Date: April 27th, 2020

DOI: https://doi.org/10.21203/rs.3.rs-23110/v1

License: This work is licensed under a Creative Commons Attribution 4.0 International License.
Read Full License

Experimental and numerical investigation of some impeller geometric parameters of an industrial electric submersible pump

Zeynel A. FIRATOGLU[a] and Mustafa N. ALİHANOGLU[b]

[a] Address for correspondence:

Department of Mechanical Engineering,

University of Harran TR- 63900, Sanlıurfa, Turkey

E-Mail: firatoglu@harran.edu.tr

[b]Address for correspondence:

Georg Fischer Hakan Plastik

Boru ve Profil San. Tic. A.S.TR- 63900, Sanlıurfa, Turkey

E-Mail: nurialihanoglu@gmail.com

Experimental and numerical investigation of some impeller geometric parameters of an industrial electric submersible pump

Abstract

Submersible pumps, which are the main means of bringing the ground liquid to the surface, are widely used in agricultural irrigation, petroleum industry, geothermal fields, and similar applications. In most applications, submersible pumps are the main energy inputs of the operating process. Therefore, a small improvement in submersible pump efficiency will significantly reduce the operating cost of the system. The motivation and focus of this study are to experimentally and numerically investigate the effect of the geometric parameters of the submersible pump on the efficiency of the pump. The submersible pump has a design in the form of the serial connection of the stages including the impeller and the diffuser and enters the multi-stage pump category. All the impeller connected to a single shaft rotates at the same angular velocity. Despite the rotation of the impeller at a constant angular speed along with the pump, the flow structure at each stage shows large variations compared to other stages. These differences lead to the formation of a complex flow structure and thus to great difficulties in the experimental identification of the flow field along with the pump. Another difficulty in the experimental definition is that the measured values can show dramatic changes depending on many parameters such as fluid viscosity-temperature, impeller inlet-outlet angle, diffuser inlet-outlet angle, number of blades, the distance between stages, surface roughness. The current general trend is to solve the above-mentioned problems with numerical simulations verified by experimental data. This trend is a result of significant developments in computer capacities parallel to the development of numerical solution methods in recent years. This trend, or the method, has been followed throughout this study. Firstly, within the scope of this study, the performance in different stages of a selected industrial submersible pump was measured by the experimental. Following the measurements, the effects of two basic geometric parameters, such as impeller outlet width and impeller outlet angle on the pump performance were examined with CFD simulations verified by the experimental measurements. This small deviation indicates that the CFD simulation results are in perfect agreement with the experimental measurements. In the simulations performed, it is observed that the time-dependent variables have their size changed but the flow structure does not change. Another striking finding from the CFD simulations carried out is; it has been observed that while geometric arrangements have a partial effect on the flow structure along with the pump, they cause a difference in the critical values on the basic variables that define pump performance, such as pressure.

KEY WORDS: Submersible pump, CFD simulations, experimental measurements, flow structure, geometric parameters

1. Introduction

Groundwater sources are the only alternative to meet the water need in agricultural areas where modern irrigation systems (canals) are not available or far from water sources. Submersible pumps are the most common means of bringing underground water resources above ground and using them in agricultural irrigation. The use of submersible pumps in agricultural irrigation stands out as the most common method in non-developed or developing countries in the Middle East, Far East, Africa, and South America, especially where modern agricultural irrigation systems are not available. In addition, in developed countries, submersible pumps are inevitably used in agricultural areas far from water sources. The biggest problem in using submersible pumps is the high energy requirement of the system. The most concrete example of this is that approximately 40 percent of the lifetime cost of the pump in a 20-year period is the energy consumed by the system**.** Another important finding is that in a study conducted by the American Hydraulic Institute, the share of pumps in total energy consumption in developed countries is 20 percent**.** As mentioned above, the share of pumps in total energy consumption in developed countries is approximately twenty percent. According to the researches, approximately 30% of this amount can be recovered with an optimal design. This result means that developed countries can save 6% of energy consumption with improvements in pumps. Therefore, the determination of optimal design parameters for pump design is extremely critical. In addition to this critical importance, as a result of the significant improvements in the size and material structure of the submersible pumps, submersible pumps are widely used in the processes of extraction of oil and natural gas as well as the need for agriculture and urban water (Zhu et al., 2016; Shi et al., 2018).

A submersible pump; is in the form of the serial connection of the stages consisting of the impeller and diffuser (Stel et al., 2015). All of the impellers connected to a single shaft rotate at the same angular speed. Although the impellers rotate at a constant angular speed throughout the pump, the flow structure in each stage differs greatly compared to other stages (Li et al., 2016). These differences cause a complex flow structure to occur and thus lead to great difficulties in the experimental definition of the flow area across the pump. Another difficulty in experimental identification is that the measurement values can vary dramatically depending on the fluid viscosity-temperature, impeller blade inlet-outlet angle, diffuser blade inlet-outlet angle, blade number, the distance between stages, surface roughness and many other parameters. The general trend recently is to solve the problems mentioned above with numerical simulations verified by experimental data. This trend is a result of significant developments in computer capacities, in parallel with the development of numerical solution methods in recent years. Accordingly, the literature studies on the subject, which include numerical and experimental processes together: (i) The relationship of geometric components with the flow field throughout the pump (Pei et al., 2016; Zhou et al., 2018; Yuanyi et al. 2009; Shi et al. 2013; Tao et al. 2017), (ii) Reliability of numerical simulations in pump design (Yao et al. 2016; Maitelli et al. 2010; Derakhshan and Nourbersi 2008) and (iii) Effect of fluid viscosity on pump performance (Zhu et al. 2016). It can be classified under three titles. These are the first two of the titles within the scope of the study. In this section, major studies are presented in order, taking into consideration the classification in question. Centrifugal pumps are tools that create a pressure gradient in the radial or axial direction as a result of an angular acceleration provided by the motor. The engineering process related to the subject can be defined as the process of ensuring the movement of the fluid through this pressure gradient with minimal pressure loss. Accordingly, there are designs related to the basic components of the pump, such as many impellers and diffusers that have been developed or are still under development. The continuation of these

development processes or the determination of the optimal design parameters will only be possible by determining the effect on the pump performance of the relation of the flow area along with the pump with the geometric parameters the effect on the pump performance. Most studies on the subject from past to present have focused on determining the relationship in question. Some of these studies are presented in detail below. Stel et al. (2015) numerically investigated the performance of a multi-stage, mixed-type submersible pump for different situations. They conducted their research in three scopes: (i) effectiveness of turbulence models in simulations, (ii) compatibility of pump operating curves obtained by numerical simulations with experimental data in the literature and, (iii) effect of distance between impeller and diffuser on the flow field. In their research, they found that, since the flow structures at each stage are significantly different from each other, and interpretation for other stages is not possible from the analysis of the flow area at any stage. Yuan-yi et al. (2009) numerically investigated the effect of the clearance between the pump flow pipe and the pump impeller on the pump efficiency and load. They conducted the research for eight different aperture values in the range of 4-18 mm and found that their maximum performance was in the 8mm aperture. *Shi et al. (2013*) investigated the effect of four different output ranges of submersible centrifugal pump impellers on pump performance numerically, theoretically and experimentally. In their study, they observed that increasing the impeller output gradually increased pump efficiency. Zhou et al. (2012) investigated the optimal design parameters for the diffuser numerically.

They performed the simulations taking into account two different diffusers and selected the pressure conversion parameter as the evaluation parameter. Yao et al. (2016) examined the effect of wall function on the results in numerical simulations that do not define the complex flow structure occurring along the pump impeller-diffuser. In their research, they selected RANS (Reynolds Averaged Navier Stokes), LES (Large Eddy Simulation) and RANS / LES hybrid turbulence models. As a result of the simulations they conducted, they found that the RANS / LES hybrid turbulence model fits the experimental data better than the other two models. Maitelli et al. (2010) numerically investigated the effect of distance between pump diffuser and impeller on pump performance curves in the submersible pump. They conducted their research within three different design conditions: (i) the current installation position of the selected pump, (ii) the distance between the pump diffuser and the impeller is zero, and (iii) the distance between the pump impeller and the diffuser is 4mm. As a result of their simulations, they observed that the minimum loss occurred in the third case. Derakhshan and Nourbersi (2008) examined the change in performance theoretically, experimentally and numerically when a centrifugal pump is used as a turbine. In their study at the best efficiency point, they detected significant deviations between experimental and numerical results.

In this study, the performance of a selected industrial submersible pump for different stages has been experimentally measured. Following the experiments, the effect of geometric parameters such as impeller output range and angle on the pump performance has been investigated numerically.

2. Material and Method

As mentioned in the previous sections, the share of pumps in total energy consumption is approximately 20%, especially in developed countries. These shares in energy consumption have made pump design one of the main engineering problems. In this engineering problem, CFD simulations are widely used in the design of new hydraulic machines or in the development of existing machines due to the difficulties in measuring the flow structure experimentally. The focus of these methods is to increase the energy efficiency of hydraulic pumps.

However, CFD simulations must be verified by experimental measurements due to the complex structure of the flow area occurring throughout the pump. In this study, experimental measurements and CFD simulations were carried out simultaneously and all simulations were verified by experimental measurements.

In this study, two impeller geometric parameters are taken into account impeller output width (IOW) and impeller outlet angle (IOA). The cross-section geometry of stage 1 of the selected industrial pump and the solid models of the impeller are shown in Figure 2.1. As can be seen from the figure, the geometric parameters taken into consideration in the studies are 15.5 mm (IOW) and 75^0 (IOA) in the existing pump. Other geometric correspondent values of the pump are given in Table 2.1. In addition to experimental measurements, a total of nine CFD simulations have been carried out, one for the existing pump geometry and the other for the impeller geometries whose geometric adjustments have been changed. The values of the four adjustments made for each of the two geometric parameters considered are given in Table 2.2.

Table 2.1. Geometrical values of the selected submersible pump.

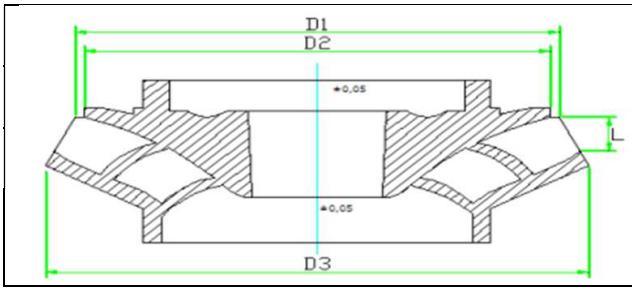

D_1	106mm
D_2	95mm
D_3	113mm
L	16mm

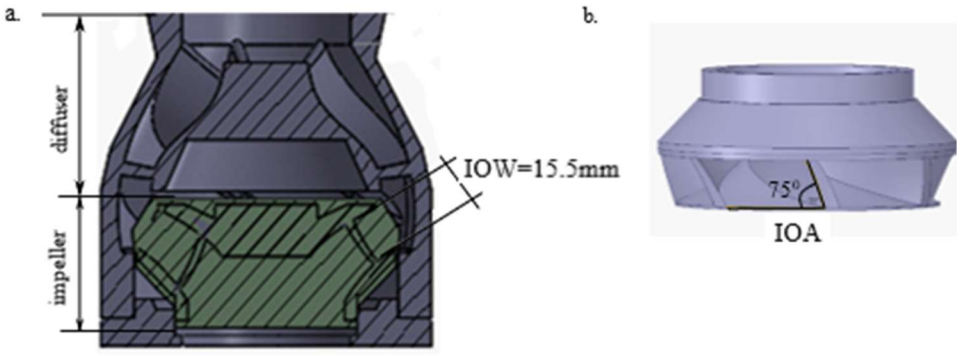

Figure 2.1. Industrial submersible pump selected as reference a. cross section, b. Impeller solid model.

Table 2.1. Geometric adjustments in CFD simulations.

	impeller output width (mm)	impeller outlet angle (^{0})
Reference Pump	**15.5**	**75**
IOW	**9.5**	75
	11.5	75
	13.5	75
	17.5	75
IOA	15.5	**80**
	15.5	**85**
	15.5	**90**
	15.5	**95**

2.1. The Basic Parameters That Define the Performance of a Pump

The performance of a pump is defined within five parameters: manometric head (*H)* flow rate *(Q*), specific energy *(n),* power *(W)* and efficiency *(η).* Working curves showing the pump performance are prepared with these parameters. Within the scope of these curves, the optimal working point is defined as the overlap point of the power and manometric head. The method followed in the extraction of the curves in question or the calculation of the five parameters mentioned above defining the pump performance will be presented below.

The flow rate that determines the required power level for the flow in fluid motion is the leading parameter in calculating pump performance. The second leading parameter that makes sense to users, in particular, is the pump suction and discharge, or the manometric pump head that defines the pressure difference between the inlet and outlet. In the literature, the delivery head is mostly indicated mWC(meter water column). It is calculated as follows;

$$H = \left(\frac{P}{\rho g} + \frac{V^2}{2g} + z\right)_{outlet} - \left(\frac{P}{\rho g} + \frac{V^2}{2g} + z\right)_{inlet} \quad (1)$$

where V, z, ρ, g are velocity, level, density, gravity respectively. The physical definition of this expression, which can be described as the extended Bernoulli or energy Equation, is in the form of the energy difference between the pump inlet and outlet. Since the inlet and outlet sections are equal in submersible pumps, from the continuity equation:

$$(VA)_{outlet} = (VA)_{inlet} \quad (2)$$

The inlet and outlet velocity are equal and the dynamic pressure difference of Equation (3.1) becomes zero. The height difference along the pump is also negligible. Therefore Equation (1) is to reduce to:

$$H = \frac{P_{outlet} - P_{inlet}}{\rho g} \quad (3)$$

As can be understood from this equation, the manometric head can be determined by the pressure difference measurements at the pump inlet and outlet. Submersible pumps are tools that convert the mechanical power, transmitted by the motor to the shaft to which the impellers are connected, to the hydraulic power. The pump hydraulic power can be defined as

$$W_{hyd} = \rho g Q H \quad (4)$$

In pumps, losses due to internal leaks, flow separations, friction, and similar processes are called mechanical losses. Mechanical losses can only be calculated by determining the shaft power. The shaft power can be calculated as:

$$W_{sh} = \omega T_{mil} \quad (5)$$

where *ω, T* are angular velocity and shaft torque respectively. Specific speed is an important parameter in pump design that can be defined as a measure of the tendencies of pump operating curves. It is calculated as follows;

$$n_q = n \frac{\sqrt{Q}}{(\frac{H}{i})^{3/4}} \quad (6)$$

Where n, *i* shows the pump rotational speed (rpm) and stage number. Specific velocity value can vary between 40 and 150 in the mixed flow pump selected in the study. After all these definitions, pump efficiency is the ratio of hydraulic power to mil power:

$$\eta_P = \frac{W_{sh}}{W_{hyd}} \quad (7)$$

In the study, the parameters mentioned above were calculated from the experimental measurements for the selected pump. The tools and equipment used in the experimental measurements will be briefly presented below.

2.2. The Experimental Setup

As mentioned, CFD simulations are widely used in determining optimal pump design parameters. However, due to the complex nature of the flow, CFD simulations must be verified by experimental measurements. In this section, the test setup used in experimental measurements will be presented. As will be understood, the experimental measurement of pump performance or operating curves is extremely critical for both designers and manufacturers. Experimental measurements were carried out in the pump test laboratory within Firat motor ve pump Electric Industry Trade Limited Company. The schematic flow chart of the test setup in which the experiments are carried out is shown in Figure 2.2. The pump head height, flow rate, effective power parameters, which were measured to determine the submersible pump characteristics, were transferred to the computer through an interface, and the pump characteristics were obtained as digital data. As can be seen in Figure 2.2, the pump is placed in the water pool in a vertical position, similar to industrial applications. Again, as can be seen from the figure, there are pressure transmitters, manometers, magnetic flowmeters and valves on the connecting pipes to measure the pressure and flow. Boards auxiliary for power and rotational speed measurement, variac transformer, network analyzers, reactive power control relay, analog ammeter are other elements of the experimental setup.

2.3 Solid Model Design of The Pump and Numerical Setup

CFD simulations were performed using commercially available CFD software ANSYS FLUENT. The Mesh design, on the other hand, is realized with icemCFD. FLUENT provides three approaches to address turbomachinery; (i) the multiple reference frame (MRF) model, (ii) the mixing plane model (iii) the sliding mesh model. Since there are unsteady flow fields in turbomachinery, the sliding mesh models the interaction with complete fidelity. Therefore, the sliding mesh approach was chosen. All flow domains and mesh designs were made in line with this selection.

Solid Model Design: Since the submersible pump or any pump consists of both moving and stationary components, the solid model cannot be formed as a single piece. The impeller and diffuser blade structure is also not suitable for drawing since it consists of different axes and is difficult to measure. This problem was solved by obtaining an optical scanning service from a company. In this process, both the diffuser and the impeller were divided into four different components in the first place. Then, all components were scanned separately, and solid models were created. In order to keep the error rate to a minimum, the solid models created were assembled in the same body, thus creating the solid model of the impeller and diffuser. The method used in the creation of solid models is a method that is widely used in the industry. In this method, two basic problems can be encountered in the form of (i) small unwanted surfaces that may occur due to the complex structure of the solid model, and (ii) incorrect joints during assembly. These problems, which may cause significant errors in numerical calculations, are solved by detailed comparisons between the selected pump components and their solid models performed by optical scanning. The selected pump components and their solid models produced by optic scanning are shown in Figure 2.3.

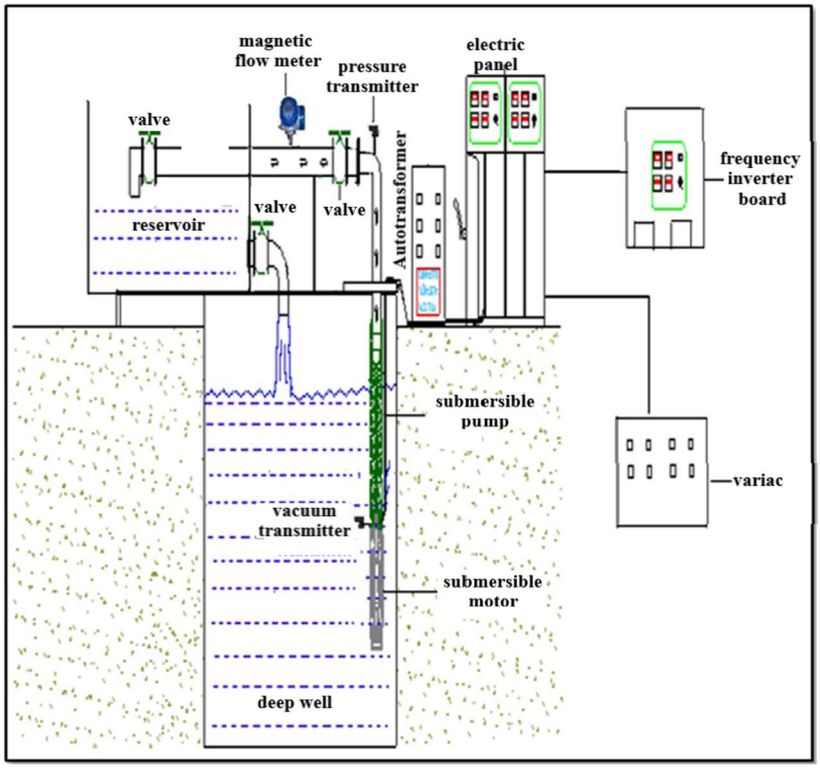

Figure 2.2. Schematic form of the experimental setup.

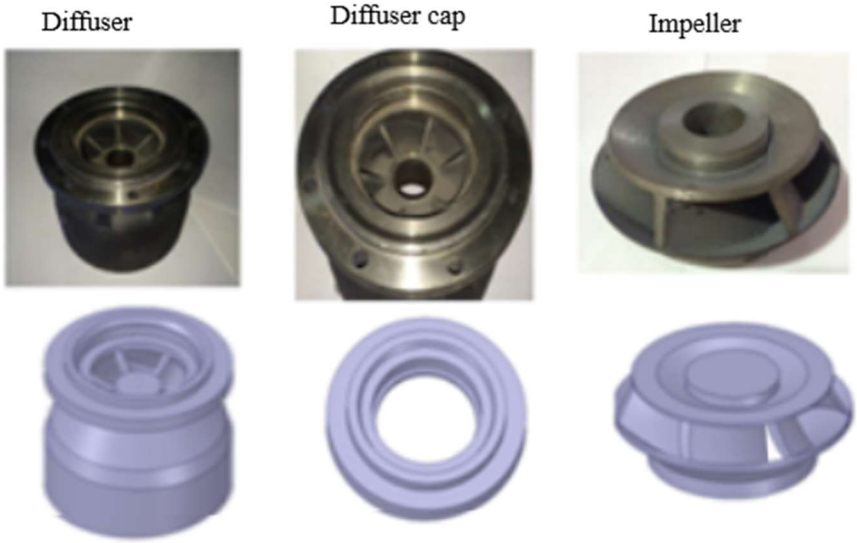

Figure 2.3. The selected pump components and their solid models produced by optic scanning.

Turbulence Model: Commercial Fluent CFD, where simulations are carried out, offers many turbulence model options such as k-epsilon, SST k-ω, Detached Eddy Simulation, Low Re k-epsilon, RNG k-epsilon. In this study, the k-ε turbulence model along with PISO algorithm was chosen in numerical simulations. Many studies in the literature have found that the k-ε turbulence model best fits experimental measurements in centrifugal pumps with reverse pressure gradient and separations (Li et al., 2016, Zhu et al., 2016, Zhou et al., 2018, Spence and Amaral-Teixeirab, 2008). Eddy viscosity in k-ε turbulence model based on two equations and Boussinesq Theorem:

$$\mu_t = C_\mu \rho \frac{K^2}{\varepsilon} \tag{8}$$

C_μ is an empirical constant. The K and ε are derived from the momentum equation. Turbulent kinetic energy (K):

$$\rho U_i \frac{\partial K}{\partial x_i} = \frac{\partial}{\partial x_i}\left[\left(\frac{\mu_t}{\sigma_K}\right)\frac{\partial K}{\partial x_i}\right] - \rho\varepsilon + \mu_t\left[\frac{\partial U_j}{\partial x_i} + \frac{\partial U_i}{\partial x_j}\right]\frac{\partial U_j}{\partial x_i} \quad (9)$$

Dissipation (ε):

$$\rho U_i \frac{\partial \varepsilon}{\partial x_i} = C_{1\varepsilon}\left(\frac{\varepsilon}{K}\right)\mu_t\left[\frac{\partial U_j}{\partial x_i} + \frac{\partial U_i}{\partial x_j}\right]\frac{\partial U_j}{\partial x_i} + \frac{\partial}{\partial x_i}\left[\left(\frac{\mu_t}{\sigma_\varepsilon}\right)\frac{\partial K}{\partial x_i}\right] - C_{2\varepsilon}\rho\left(\frac{\varepsilon^2}{K}\right) \quad (10)$$

In equations, σ_K, σ_ε, $C_{1\varepsilon}$, $C_{2\varepsilon}$, and C_μ are model constants. In the simulations, these constants were selected as 1, 1.3, 1.44, 1.92 and 0.09, respectively.

Computational domain and Mesh Design: Flow field was designed by using solid models created as a result of optical scanning. The designed flow domains are shown in Figure 2.4. As can be seen from the figure, in addition to the impeller (rotating)and diffuser (stationary) flow domains, in order to reduce the errors that may occur on the simulation results due to possible pressure fluctuations in the pump inlet-outlet, a certain length of connection pipe is installed at the pump intake and discharge domains.

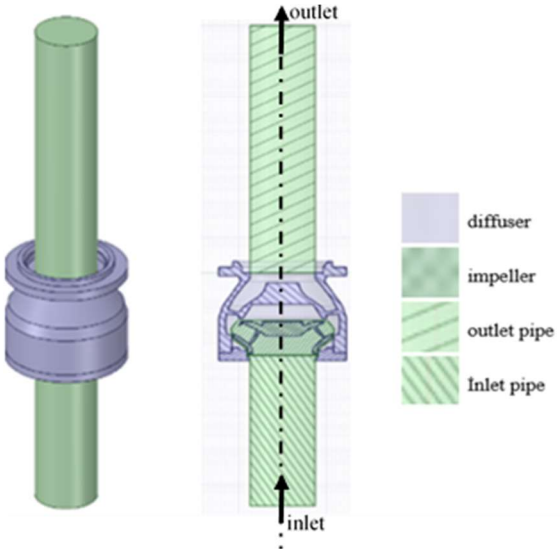

Figure 2.4. Computational domains.

The primary parameter considered in the mesh design in a flow field is the laminar sublayer, which is one of the basic parameters that occur in the turbulence boundary layer and defines the relationship between the flow and the solid surface. The value of y^+ in the region in question is between 1-5. The numerical calculation process can only be defined by the fact that several node points are located in this region. The mesh design to be made by leaving a few nodes in the laminar sublayer significantly increases the calculation load and time. In engineering applications, it is generally preferred to define the laminar sublayer region with mathematical models called wall function and to decrease the calculation load and time. The wall functions were defined as follows:

$$U^+ = \frac{1}{K} log y^+ + B \quad (11)$$

Where *B* and *K* are dimensionless numbers that vary depending on the turbulence model. U^+ *and* y^+ *in the* equation are respectively; $U^+ = U_0/\sqrt{\tau/\rho},\ y^+ = y\sqrt{\tau/\rho}//v.$ In addition, $U_0,\ \tau, v$ *and* y are the mean velocity, shear stress, kinematic viscosity, and the length of the first joint from the surface respectively. In simulations, standard wall functions are applied for near-wall treatment.

In this study, the design parameter considered in accordance with the turbulence model selected in the mesh design is to provide y + <11 at the first node point from all surfaces. Using the automatic mesh feature of the package program selected in the first place considering the mentioned criterion, mesh design was made with elements having tetrahedron in the flow fields. Based on the criteria considered in the next step, local mesh increments were made. As a result of the simulations carried out after the first mesh design, when y^+ did not reach the desired values, the number of mesh was increased 9.5% and 13% in the areas close to the solid surfaces of the impeller and diffuser respectively, In the simulations repeated after mesh increments, in the impeller and diffuser inlet-outlet areas with high pressure and velocity gradients, the y^+ value ranged from 43 to 150. On top of that, mesh increments were made at the rate of 20%, 17%, 19% and 13% respectively to the impeller inlet, impeller outlet, diffuser inlet and diffuser outlet. As a result of the simulations made after this operation, the y^+ value remained below 11 in the first node points on the surfaces. At the end of these processes, the mesh structure of the designed impeller and diffuser surface is shown in Figure 2.5.

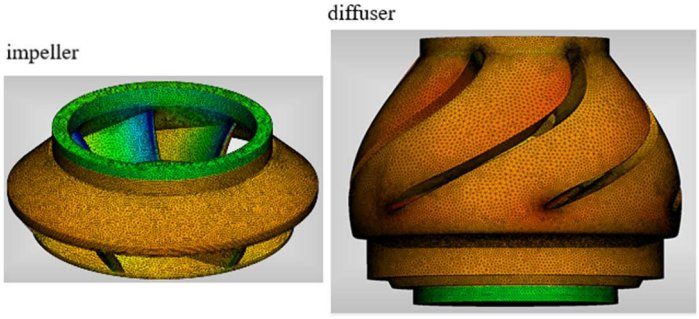

Figure 2.5. Impeller and diffuser mesh design.

Boundary conditions: The fluid used in the numerical simulation and experimental investigation is water and the density of 1000 kg/m3 and kinematic viscosity of 1.02 mm2/sn at 25 0C. In the present numerical simulations, the flow field were defined by four numerical domains, one of which is rotating (impeller), three of which are static (diffuser, intake and discharge pipes). After all numerical domains are transferred to fluent, they were connected by interfaces. In this study, boundary conditions are determined by considering the maximum operating point of the pump selected. The selected pump has a flow rate of 15 lt/sn at the maximum operating point at 2900 rpm. In accordance with the experimental measurements, the flow rate (15 lt/sn) was applied to the outlet boundary of flow fields while pressure-inlet (total pressure, gauge Pressure, 0 Pa) was applied to the inlet. The non-slip boundary condition ($\frac{\partial u_i}{\partial x_i} = 0$) was selected to all solid surfaces in the flow fields. In the simulations, the rotating domain(impeller) was selected at 2900 rpm in accordance with the experimental measurements. In the simulations, the solution time steps, which are selected as time dependent flow, were calculated by taking into account the rotational speed of the rotating region. The timestep of the unsteady calculations was set $1.724*10^{-4}$ s. The timestep was related to the rotational speed, such that each timestep represented an increment in angular rotation of 3 deg.

3. **Results and discussion**

Within the scope of this study, the performance of a referenced industrial submersible pump at different stages was first measured by the experimental set and measurement tools presented in the previous section.

Following the measurements, the effect of four different values of the impeller output width and angle on the pump performance was examined with CFD simulations confirmed by experimental measurements. In this section, the results of the experimental measurements and CFD simulations conducted throughout the study will be presented with detailed graphs and numerical data. Accordingly, experimental measurement data will be given in the first place. After the presentation of the experimental data, the simulation data carried out regarding the effect of the impeller output width and angle on the pump performance will be presented. Finally, experimental measurement data and CFD simulation results will be evaluated together

3.1. Experimental Measurements

The industrial submersible pump, which is taken as reference in the study, is supplied to the industry by the company with a motor with 9-stages and 25 hp power. Performance measurements of the pump in question were carried out at 2900 rpm in 9, 5 and 1 stages, respectively.

Depending on the flow rate measured with the 9-stage construction of the referenced pump, the changes in the pump delivery head, pump and system efficiency are shown in Figure 3.1 (a). As can be seen from the figure, in accordance with the literature (Wang et al. (2013), Makteli et al. (2010)), the pump delivery head and the efficiency curves show a parabolic trend.

It measures the flow rate of 7.55 lt /sn at 111.1 mCW maximum head. At this point, the efficiency of the pump is 14% while the efficiency of the system is 13%. The minimum pump delivery head is measured as 9.1 mCW and the flow rate at this point was determined to be 23.17 lt /sn. At this point, the efficiency of the pump is 50% while the efficiency of the system is 45%. In the measurements made, it has been determined that the maximum pump efficiency is 69%. At this point, the pump delivery head is 84.7mSS and the flow rate is 15.1 lt /sn. Therefore, hydraulic power is 12.556 kW at the optimal working point determined. Also, at this point, while the efficiency of the pump is 69%, the efficiency of the system is 63%. After this point, both pump efficiency and system efficiency decrease dramatically.

Within the scope of this study, a 15 hp engine was used in the measurements for 5 stages. As mentioned above, the measurements were taken at 2900 rpm of the motor. Depending on the flow rate measured for this construction, the changes in the pump delivery head, pump and system efficiency are shown in Figure 3.1 (b). As can be seen, both the delivery head and efficiency curves show a parabolic trend. It measured a flow rate of 7.55 lt/sn at 61.345 mCW maximum pump delivery head. At this point, the pump efficiency is 51.35%, while the system efficiency is 45.23%. The minimum pump delivery head is measured as 5.05 mCW and the flow at this point is determined to be 61.34 lt/sn. At this point, the efficiency of the pump is 13.75%, while the efficiency of the system is 12.8%. In the measurements taken, the system efficiency with the maximum pump is 67.201% and 59.02% respectively. At this point, the pump delivery head is 47.118 mCW, while the flow rate is 15.3 lt/sn. In addition, the hydraulic power at this point was calculated as 7.072 kW. The pump decreases approximately by 1.8% in pump efficiency and 4% in system efficiency compared to 9 stages at the maximum operating point.

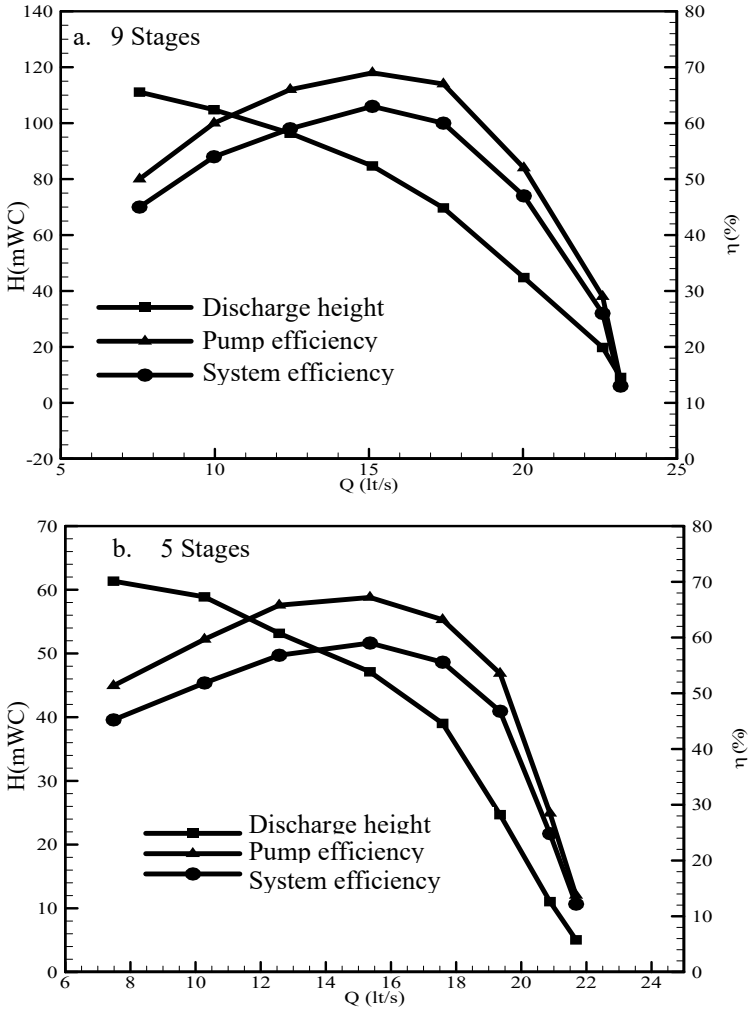

Figure 3.1. Operating curves of (a) the 9-stage and (b) 5 stage submersible pump.

In the experimental measurement processes of the 1-stage pump, 4 hp motor was used. The pump operating curves prepared as a result of the measurements made are shown in Figure 3.2(b). As can be seen from the figure, depending on the flow rate, the pump delivery heads, pump and system efficiency show a third-degree parabolic trend similar to 9 and 5 stages. The motor speed is set to 2900 rpm, similar to the measurements for 9 and 5 stages. In the measurements made, it was observed that the flow rate was 7.25 lt/sn when the maximum delivery head was 12.34 mCW. At this point, the pump efficiency is 51.5% while the system efficiency is 42.52%. When the flow control valve is fully open, the minimum delivery head is measured as 1.05 mCW and the flow rate at this point is determined to be 21.89 lt/sn. At this point, the efficiency of the pump is 13.44%, while the system efficiency is 11.45%. In the measurements taken, the system efficiency with the maximum pump is 66.24% and 55.48% respectively. At this point, the pump delivery head is 9.35 mCW and the flow rate is 15.4 lt/sn. In addition, the hydraulic power at this point was calculated as 1.412 kW.

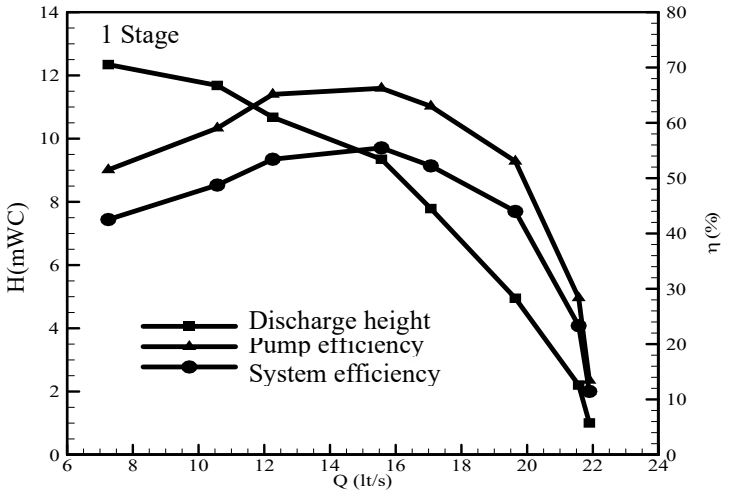

Figure 3.2. Operating curves of 1 stage submersible pump.

Another important detail observed in the measurements made is the relationship of the ratio of pump efficiency to system efficiency with the number of stages. In order to define this relationship, the ratio of pump efficiency to system efficiency was calculated along the working curves for all stages measured. As a result of the calculations, the change of the pump efficiency to the system efficiency for the measured stages along the pump operating curve is shown in Figure 3.3. As can be seen from the figure, the system efficiency in 9 stages approaches the pump efficiency compared to other stages. Due to the decrease in the number of stages, the said ratio was growing. Along the pump operating curves for all stages, except when the maximum the pump discharge pressure is minimum the ratio of pump efficiency to system efficiency reaches its lowest value at the maximum operating point of the pump. For example, in the 9-stage pump, the ratio at the maximum working point is 1.095, while the previous and next points are 1.118 and 1.116, respectively. In the 1-stage pump, the ratio in the maximum working point is 1.193, while the previous and next points are 1.22 and 1.206, respectively.

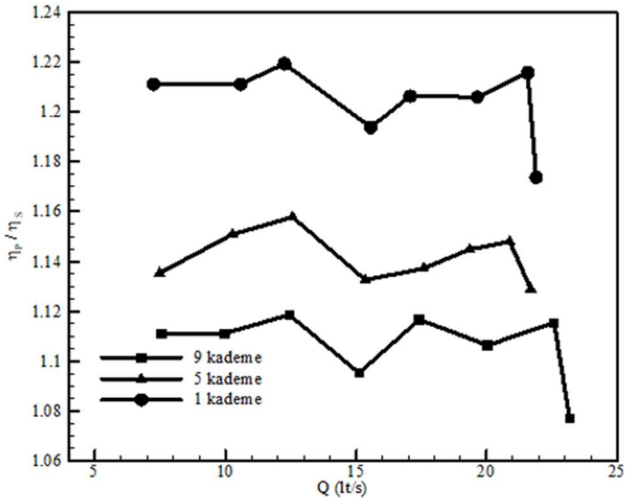

Figure 3.3. The rate of the pump efficiency to the system efficiency (η_p / η_s) in the measured stages depending on the flow rate.

3.2. Effect of Mesh Count on CFD Simulation Results and Verification of Simulations with Experimental Data

Within the scope of the study, mesh design is the most critical process in terms of the reliability of the processes followed in the CFD simulations carried out. As mentioned before, it is imperative to make the mesh

design of a flow field within the framework of the selected turbulence model and wall function. In this study, the mesh design of the flow areas was made by taking into consideration the necessity mentioned. In the first trial simulations, y+ values recommended were reached for the selected turbulence model. Another parameter that determines the reliability of a CFD simulation is to reach a solution independent of mesh. In order to provide this parameter, the mesh numbers determined as a result of the mesh design process are designed in three different mesh structures, mostly in areas close to solid surfaces, 10% reduction, 10% and 20% increase. The effects of mesh count on simulations were examined with CFD simulations carried out within the framework of the different mesh structure.

For the different mesh counts mentioned above, it was found that in CFD simulations carried out under the same boundary conditions, the number of mesh had a very limited effect on the sizes defining the flow area, but did not change the flow structure. This situation can be clearly seen from Figure 4.6, where the pressure distribution and streamlines are prepared as a result of the simulations carried out for four different mesh count or densities for a 1-stage pump. As can be seen in Figure 3.4, a similar flow structure is observed in every four mesh count. In addition to this similar flow structure, the deviation in pump delivery head, which is critical in determining the pump performance, in the 10% and 20 mesh count increments, the deviation remains between 1-2%, while the 10% reduction deviation is 2.3%. These similar flow structures and low deviation values show that the simulation results are independent of mesh.

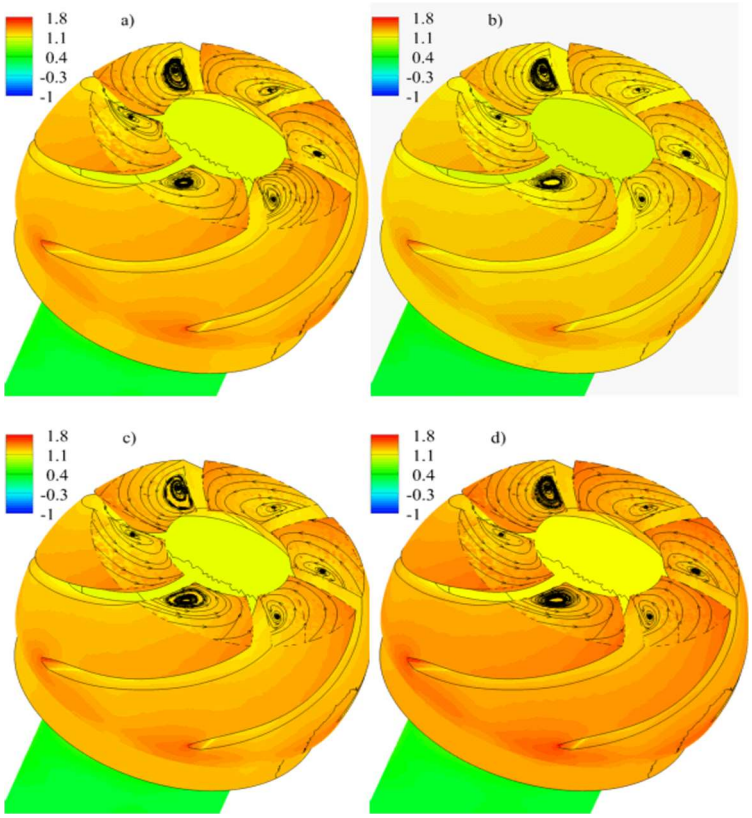

Figure 3.4. Pressure distribution (mCW) and streamlines a) 8700233, b) 1.1*8700233, c) 1.2*8700233 ve d) 0.9*8700233 mesh count.

In the current criteria of the selected industrial pump, CFD simulation was carried out for 1-stage pump at 15 lt/sn flow rate and 2900 rpm boundary conditions. It can evaluate the purpose of CFD simulations carried out at this phase in two classes: (i) to measure the reliability of the simulations to be carried out in the next stages by

reference to the experimental data and (ii) in the next steps, to reach the required data to compare the simulations to be carried out for 8 different geometric parameters with the current pump.

Throughout this study, in all CFD simulations carried out, graphs showing the pressure distribution and streamlines in detail were prepared in order to define the flow structure. As a result of the simulation carried out for the 1-stage pump for the current criteria of the pump selected at this phase, the pressure distribution and streamlines throughout the pump are shown in Figure 3.5. While the pressure increases dramatically through the impeller from the inlet, after the impeller exit, the increase and decrease in pressure was remain within very limited ranges. The pressure at the impeller inlet is approximately 3.27 mCW. At the exit of the impeller, the pressure increases by 1.75 times and reaches 9.18 mCW. At the impeller outlet or diffuser inlet, the pressure immediately reaches about 9 mCW, and then the pressure fluctuates in 9-9.8 mCW intervals. Although pressure reaches approximately 9.76 mCW throughout the diffuser, pressure close to the diffuser outlet immediately reaches 9.1mCW. In a remarkable finding, a low-pressure zone is formed approximately 1.1 mCW lower than the environment in the flow area just above the diffuser outlet. As can be seen from streamlines in Figure 3.5. (b), the low-pressure zone in question is the main parameter that determines the flow structure after the diffuser outlet. In the said low-pressure region, a reverse vortex is observed on the side of the pump center axis. On the other side of the same low-pressure zone, another vortex system, which is much smaller in proportion, is formed. As can be seen in Figure 3.5. (b), the main parameter that determines the flow structure in the diffuser outlet zone is the two vortex systems mentioned. In the examinations made again, considering the pressure distribution, the flow structure at the diffuser outlet continues in the next flow fields. As will be understood, the region where the relationship between pump performance and flow structure can be best defined is the flow area at the diffuser outlet. Another remarkable finding is the increasing tendency of the pressure from the center to the outside.

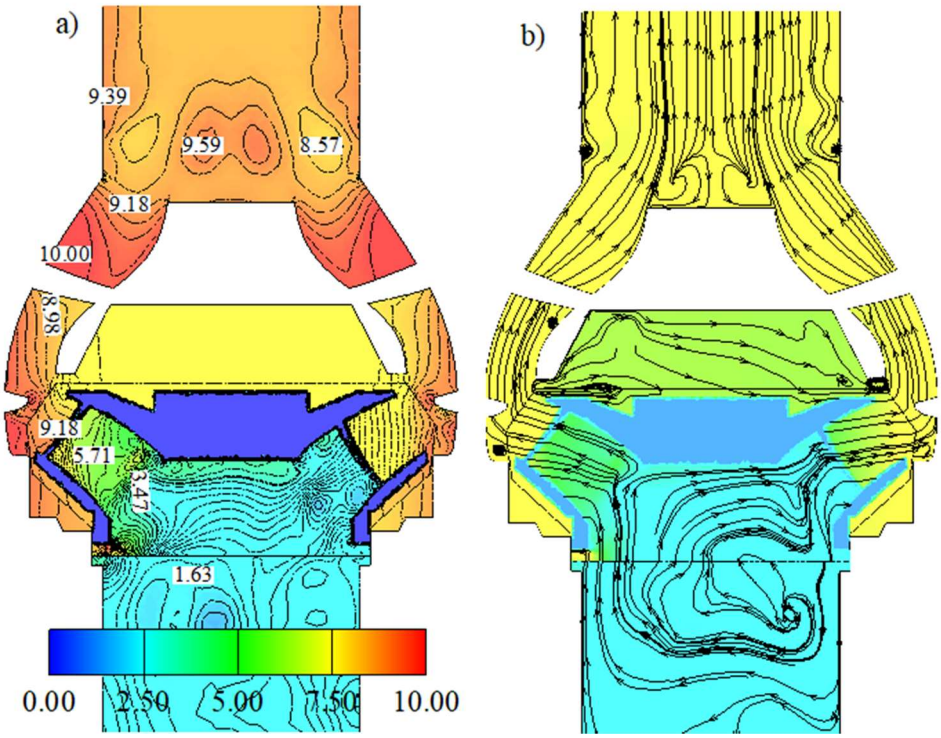

Figure 3.5. As a result of the CFD simulations of the 1-stage pump in the current criteria of the selected pump, a) pressure distributions, b) streamlines

As a result of the CFD simulation carried out for the 1-stage pump, the pump delivery head was calculated as 8.65 mWC and the pump efficiency was calculated as 67.2%. When these results are compared with the experimental measurements, the deviation rates from the experimental measurement data are 8% at pump delivery head and 1.5% at pump efficiency. The reason for the large deviation in the delivery head compared to the pump efficiency is that in the CFD simulation, the flow rate is chosen as a fixed limit condition of 15 lt/sn. However, in experimental measurements, the flow shows oscillations in the range of 15-15.3 lt/sn.

3.3. Effect of Impeller Output Width on Pump Performance

One of the most important geometric parameters that determine flow characteristics throughout the submersible pump is the impeller output width. The flow structure along with the pump and the effect of these structures on the pump performance for four geometric values, different from the impeller output width (15.5mm) of the selected industrial pump was investigated with CFD simulations at the same boundary conditions. The geometrical dimensions considered are 9.5, 11.5, 13.5 and 17.5mm, respectively, with reference to the impeller output range in the simulations. As can be understood from the given values, it is aimed to define the effect of 2mm increase or decrease in the impeller output range on the pump performance. In the CFD simulations carried out, it has been determined that the impeller output width has a partial effect on the flow structure throughout the pump,

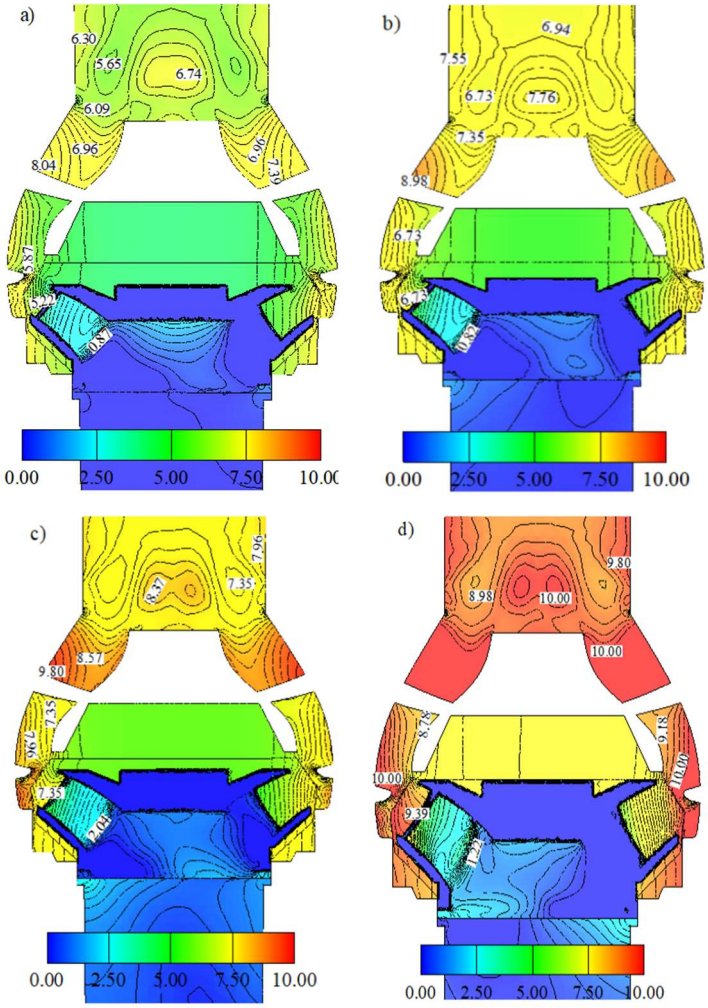

Figure 3.6. Pressure distributions throughout the pump for a) 9.5 mm, b) 11.5 mm, c) 13.5 mm and d) 17.5 mm values of impeller output width.

while it causes a difference in significant scales on the basic variables that define pump performance such as pressure. This can be clearly seen from Figure 3.6, where pressure distributions are shown for four different values of said impeller output width. As can be seen from the figure, the increase in pressure for the values of 9.5, 11.5, 13.5 and 17.5mm of the impeller output width along with the impeller is 4.4, 5.86, 6.2 and 8.14 mWC, respectively. The pressure increased gradually throughout the diffuser at all four impeller output width geometric values along the diffuser and, the maximum pressure value along the diffuser for the geometric values of 9.5, 11.5, 13.5 and 17.5 mm of the impeller output width was found to be 8.04, 8.98, 9.8 and 10 mWC, respectively. Low-pressure zones were observed at the diffuser outlet for all four geometric values. In addition, maximum pressures in all four geometric values occurred in the outer wall of the diffuser blades. Another of the observations made is that the impeller output width, where the flow regions are most obvious, is 17.5 mm, with the reference of pressure. The clearest removable finding in Figure 3.6 is that the pump delivery head changes significantly as the impeller output width changes.

From the CFD simulation data carried out for four different impeller output width, pump delivery head, torque, hydraulic force in the vertical direction and pump efficiency have been calculated as numerical values. As a result of the calculations, the effect of the impeller output width on the pump delivery head and efficiency is shown in Figure 3.7. The figure also includes the value of the pump delivery head and efficiency at 15.5 mm, which is the impeller outlet range of the currently selected pump. As can be seen from the figure, the pump delivery head is approximately 6.36 mWC, when the impeller outlet width is 9.5mm, while it is 9.15 mWC when the impeller outlet width is 17.5mm. An increase of 8mm in the impeller output range increases the pump delivery head by approximately 43%. Another important finding that can be clearly understood from Figure 3.7 is that the most dramatic increase in pump delivery head occurs when the impeller output width increases from 13.5 to 15.5mm. In this increase, the pump delivery head reaches approximately from 7.19mWC to 8.64mWC or the increase is approximately 20.16%.

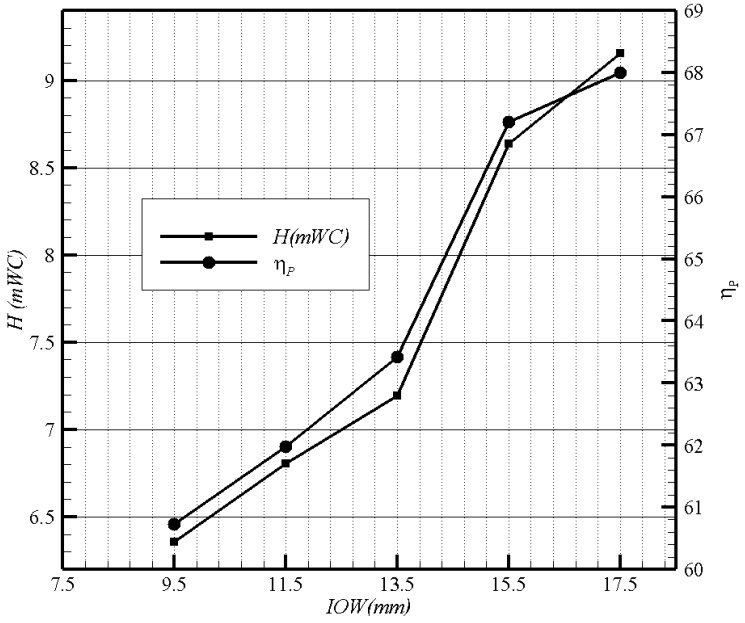

Figure 3.7. Effect of impeller output width on pump delivery head and efficiency.

The most important parameter in the choice of the pump in terms of operation or end-user is pump efficiency. As can be seen from Figure 3.7, as the impeller output width expands, the pump efficiency increases at a certain rate. For example, the pump efficiency is 60.73% for the 9.5mm impeller output width and 68% for the 17.5mm. The most dramatic increase is in the 13.5-15.5 mm impeller output width range with 3.78%. In other ranges, the rate of increase in yield remains below 1.5%.

While any fluid moves on a solid surface, it causes shear stress on the solid surface due to its dynamic pressure, while it causes normal stress due to static pressure. Cracks occurring on the solid surface in contact with the fluid are often the source of said normal stress. The hydraulic force, which causes the mentioned normal stress and caused by static pressure, may cause vibrations during pump operation and significantly decrease pump life (Li et al., 2017). In all CFD simulations carried out in this study, the hydraulic force coming to the impeller in the vertical direction was calculated. Because, as expected, the biggest pressure difference occurs between the impeller output and inlet throughout the pump, therefore the hydraulic force reaches maximum values in this region.

The effect of the change in the impeller outlet width on the hydraulic force and pump torque is shown in Figure 3.8. As can be seen from the figure, the torque value for the 9.5mm impeller output width is 5.072Nm, while the torque for the impeller output width of 17.5mm is 6.524 Nm. An increase of 28.62% of torque occurs in the 9.5mm to 17.5mm impeller output range. The most dramatic increase in torque occurs at 13.3% in the range of 13.5mm to 15.5mm, as is the pump delivery head. This increased value is 4.89, 3.31 and 4.77% for the impeller output width of 9.5-11.5, 11.5-13.5 and 15.5-17.5 respectively. As can be seen, in the 3.5 to 15.5 mm impeller output range, the increase in torque is more than double compared to other ranges. The increase rate provided by the increase in the impeller output width at the pump delivery head was remained at a lower level in the torque value to be clearly seen.

As can be seen from Figure 3.8, the hydraulic force for the 9.5mm impeller output width is 189.6 N, while it is 206.67 N for the 11.5mm impeller output width. The most interesting finding is that the hydraulic force reaches a minimum value of 178.92 N outside the general trend for the 13.5 mm impeller output width. When the 13.5mm impeller output width value is increased by 2mm, that is 15.5mm, the hydraulic force increases by approximately 27% and becomes 227.203 N. For example, when the impeller output width is increased from 9.5mm to 11.5mm and 15.5mm to 17.5mm, the increase in hydraulic force is 9 and 10% respectively. This determination shows that the impeller output width has a direct effect on the hydraulic force. Another important striking observation that can be observed from Figure 3.8 is that there is an optimal point where the hydraulic force is minimized for a given impeller output width.

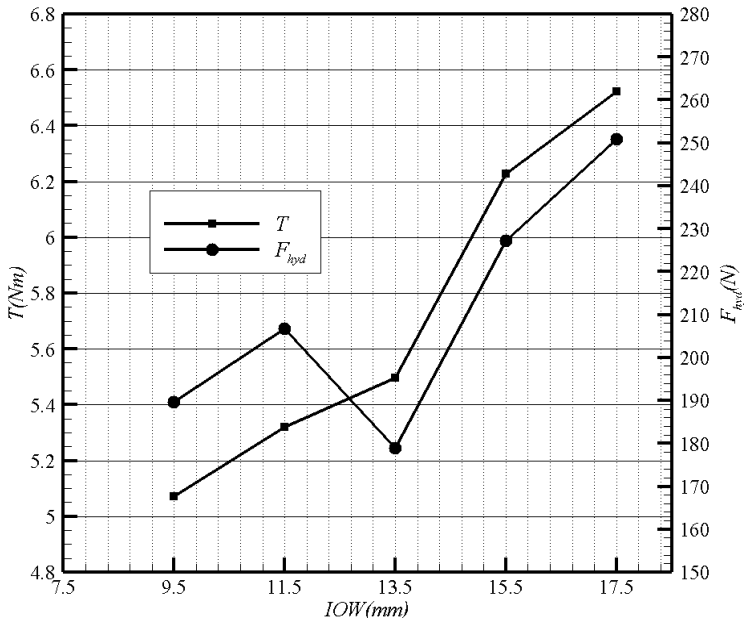

Figure 3.8. Impact of impeller output width on pump torque and the hydraulic force.

3.4. Effect of Impeller Output Angle on Pump Performance

Another geometric parameter considered in this study is the impeller output angle. The impeller output angle of the existing industrial pump, which is referenced, is 75^0. Besides this impeller output angle, CFD simulations were carried out in four different impeller output angles, 80^0, 85^0, 90^0 and 95^0. In the CFD simulations carried out, it was observed that increasing the impeller output angle compared to the existing pump had a very limited effect on the flow structure while having a significant effect on the pressure distribution throughout the pump. This determination can be clearly observed from Figure 3.9, where the pressure distribution across the pump is shown for four different impeller output angles.

As can be seen from the figure, the pressure increases from 1.25 mWC to 7.35mWC for the impeller output angle of 80^0. The increase in pressure is about 6.1mWC. Although pressure reaches 9.18mWC throughout the diffuser, the pressure drops 7.96 mWC at the diffuser outlet. Also, a pressure zone of approximately 0.7mWC lower than its surroundings occurs immediately after the diffuser outlet. The pressure rises from 2.81 mWC to 7.81 mWC along with the impeller at the 85^0-impeller output angle. The increase in pressure is approximately 6 mWC. Although 9.06 mWC through the diffuser, the pressure drops to 7.81 mWC at the diffuser outlet. Another finding observed is the low-pressure zone occurring immediately after the diffuser outlet. As can be seen, the pressure followed by the increase or decrease trend along with the pump shows a trend similar to the two impellers output angles mentioned above. This trend is also in question at 90^0 and 95^0 impeller output angles. For example, at 950 impeller output angle, pressure increases from 0.77 mWC to 1.15 mWC along with the impeller. The pressure increase rate along the impeller is approximately 49%. For these two impeller output angles, the trend in pressure after the impeller shows a similar trend with the two impeller output angles presented above as numerical data. As can be clearly seen from Figure 4.17, although the pressure distribution after the impeller shows a similar tendency at all impeller output angles, the increase or decrease rate changes significantly. It has been observed that the pressure increase rate decreases especially as the impeller output angle increases.

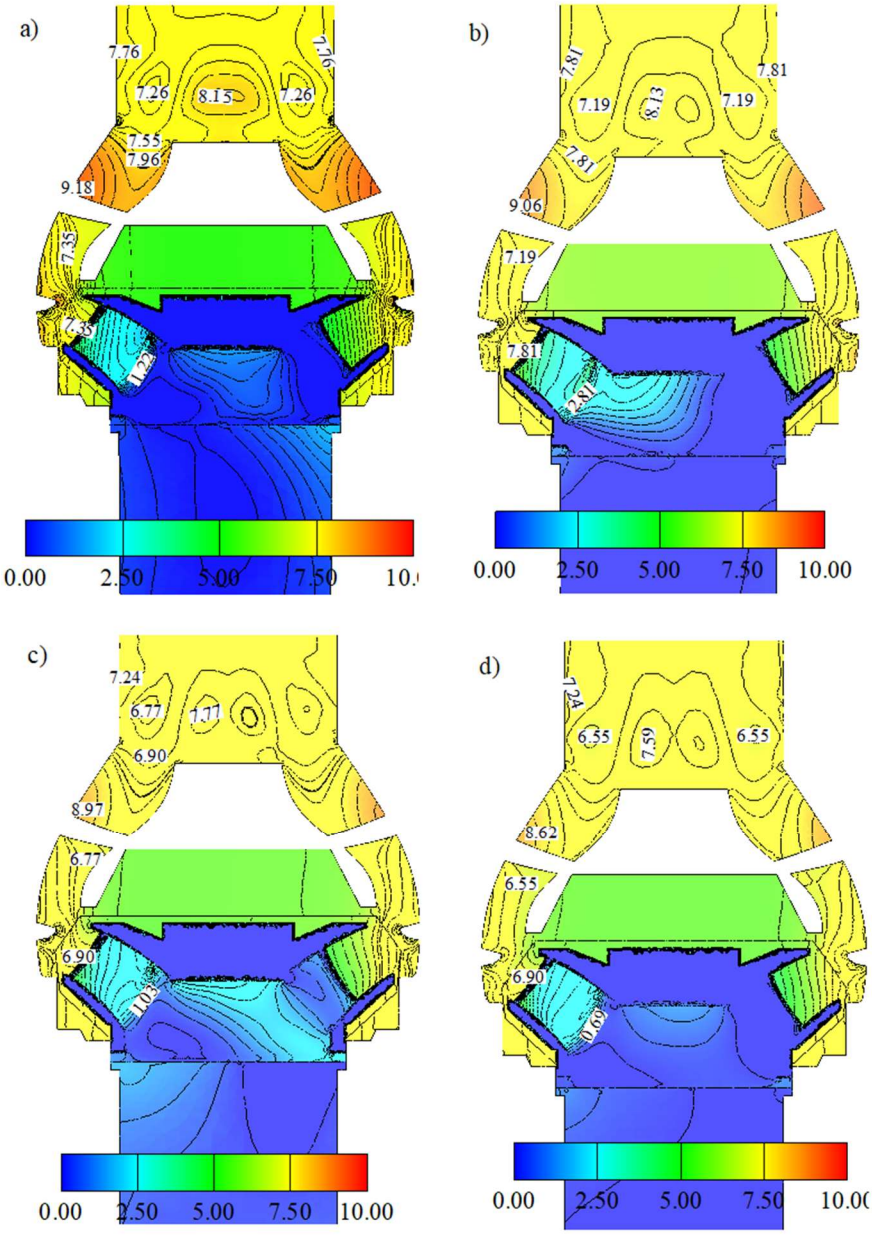

Figure 3.9. Pressure distributions throughout the pump for a) 80^0, b) 85^0, c) 90^0 and d) 95^0 values of impeller blade angle.

In the CFD simulations carried out, it has been observed that as the impeller output angle increases, the pump delivery head and its efficiency decrease. The change in pump delivery head and efficiency depending on the impeller output angle calculated as a result of CFD simulations is shown in Figure 3.10. As can be seen from the figure, 75^0 pump delivery head, which is the impeller outlet angle of the selected industrial pump, is 8.636 mWC, while it is 7.79 mWC at the 95^0 impeller outlet angle. Therefore, the pump delivery head decreases by 10.86% in 200 increases of the impeller blade angle compared to the current situation. As can be clearly seen from Figure 3.10, the pump delivery head decreases by approximately 2% when the wing outlet angle increases from 50 starting from 75^0, while the amount of falling in subsequent increases is above 3%. Changing any geometrical parameter throughout the pump affects the changing of flow volumes, thus the process of converting mechanical power into hydraulic power, positively or negatively. In the simulations carried out, it has been observed that the impeller output angle does not have a significant effect on the pump torque, which is an indicator of mechanical

power. As a result of the simulations, the pump torque and hydraulic force according to the calculated impeller output angle are shown in Figure 3.11. As can be seen from the figure, the increments of the impeller output angle 5^0 have no significant effect on the pump torque. Changing the impeller outlet angle causes limited changes in pump torque in the range of 6.149-6.227 Nm as mentioned above. As can be seen from Figure 3.11, there is no apparent trend in hydraulic force as a result of 5^0 increases in the impeller output angle. For example, when 75^0 impeller output angle 80^0 is subtracted, the hydraulic force decreases by 4.65% and when it is increased from 80^0 to 85^0, hydraulic force increases by 11.29%. The most dramatic drop occurs in 16% when the impeller output angle is subtracted from 85^0 to 90^0. The most dramatic increase in hydraulic force has occurred with 16.71% when the impeller wing angle is subtracted from 85^0 to 90^0. As can be understood from the findings mentioned above, the arrangements in the impeller output angle have a limited effect on both the pump torque and the hydraulic force. In the calculations made from the CFD simulation results carried out compared to this limited effect, the effect of the impeller blade angle on the pump efficiency was found to be significant. As can be seen in Figure 3.10, while the pump efficiency is 67.2% at 75^0 impeller output angle, when the impeller blade angle 95^0 is subtracted, the pump efficiency drops to 60.86%. The decrease is approximately 10%. The most dramatic drop is experienced with 3.9% when the impeller output angle is subtracted from 90^0 to 95^0.

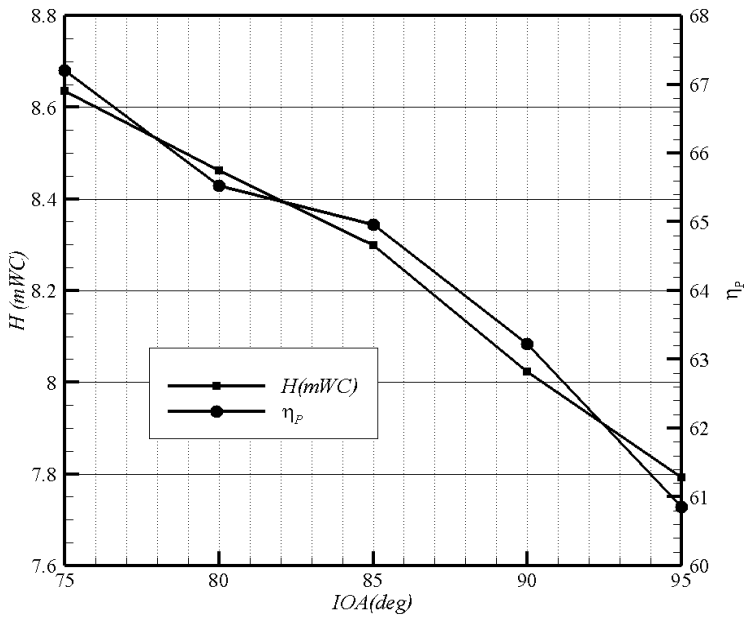

Figure 3.10. Effect of impeller output width on pump delivery head and efficiency.

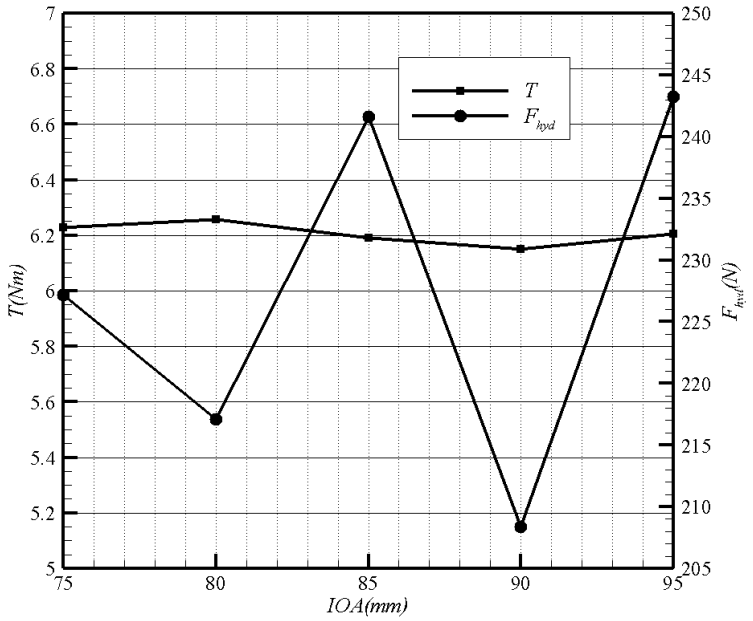

Figure 3.11. Impact of impeller output angle on pump torque and the hydraulic force.

4. Conclusion

The effect of two basic impeller geometric parameters (impeller output width and angle) of a selected industrial submersible pump on the pump performance of the four different states for each was investigated by CFD simulations confirmed by experimental measurements. Within the scope of the study, the effects of 9 scenarios on pump performance with CFD simulations were investigated for four different criteria of each geometrical parameter mentioned above. Before CFD simulations, pump performance was measured experimentally at the 1, 5 and 9 stages of the selected industrial pump. In the measurements made, it has been observed that the number of stages has a small effect on the pump efficiency. Another striking finding is that the impact of the number of stages over the system efficiency is remarkable compared to this relative effect. Simultaneously with the experimental measurements, it conducted CFD simulation for the 1-stage pump in the geometric criteria of the selected pump and within the limits of the experimental measurements. In the studies carried out, it was observed that the CFD simulation results were in full agreement with the experimental measurements. For example, the pump efficiency calculated as a result of CFD simulations in a single-stage pump showed 1.5% deviation from the experimental measurements. This result is the leading parameter showing the reliability of the method followed in the execution of CFD simulations. The findings obtained as a result of the simulations carried out below are given in summary form:

Impeller output width: Observed from the pump efficiencies calculated as a result of the CFD simulations carried out, as the impeller output width expands, the pump efficiency increases at a certain rate. For example, the pump efficiency is 60.73% for the 9.5 mm impeller outlet range, while it is 68% for 17.5 mm. A similar trend has been observed in pump delivery head and torque.

Impeller output angle: It has been determined that the arrangements in impeller output angle have a limited effect on both pump torque and hydraulic force. It has been determined that the impeller output angle has a significant effect on the pump efficiency compared to this limited effect. As a result of the calculations, while the pump

efficiency is 67.2% at 750 impeller output angle, the impeller output angle is removed 950, the pump efficiency decreases to 60.86%. The decrease is approximately 10%.

List of Figure Captions

Nomenclature

D diameter (m)

F_{hyd} hydraulic force (N)

g gravitational acceleration (m/sn^2)

H head (mWC)

i stages number

IOA impeller output angle (deg)

IOW impeller output width (mm)

k turbulent kinetic energy (m^2/sn^2)

P pressure (Pa)

Q volumetric flow rate (m^3/s)

T torque (Nm)

U_0 mean velocity (m/sn)

v kinematic viscosity (m^2/s)

V velocity (m/s)

W power (W)

y^+ dimensionless wall distance

z level (m)

Greek symbols

ω angular velocity (rad/sn^2)

ρ density (kg/m^3)

ε Dissipation

η_P pump efficiency

η_S pump efficiency

μ_t eddy viscosity

Subscripts

hyd hydraulic

mil mil

o mean

p pump

S system

sh shaft

t turbulent

Declarations

Availability of data and materials

- The datasets used and analyzed during the current study are available from the corresponding author on reasonable request.
- All data generated or analyzed during this study are included in this published article.

Competing interests

- The authors declare that they have no competing interests

Funding

- There is no funding source in conducting the research.

Authors' contributions

- ZAF carried out CFD simulations and interpreted experimental and numerical data.
- MNA, preparation of the experiment set, taking measurements and was a major contributor in writing the manuscript.

Acknowledgements

- Not applicable

Authors' information

- Not applicable

References

Derakhshan, S., Nourbakhsh, A. (2008). Theoretical, numerical and experimental investigation of centrifugal pumps in reverse operation. Experimental Thermal and Fluid Science, *32* (8), 1620-1627. DOI: 10.1016/j.expthermflusci.2008.05.004

Li, J. W., Zhang, Y. N., Liu, K. H., Xian, H. Z., Yu, J. X. (2017). Numerical simulation of hydraulic force on the impeller of reversible pump turbines in generating mode. Journal of Hydrodynamics, 29 (4), 603-609. https://doi.org/10.1016/S1001-6058(16)60773-4

Li, W., Jiang, X., Pang, Q., Zhou, L., Wang, W. (2016). Numerical simulation and performance analysis of a four-stage centrifugal pump. Advances in Mechanical Engineering, 8 (10), 1-8. https://doi.org/10.1177/1687814016673756

Maitelli, C. D. P., Bezerra, F. V. M., Mata, W. (2010). Simulation of flow in a centrifugal pump of esp systems using computational fluid Dynamics. Brazilian journal of petroleum and gas, 4 (1), 1-9.

Pei, J., Wand, W., Yuan, A., Zhang, J. (2016). Optimization on the impeller of a low-specific-speed centrifugal pump for hydraulic performance improvement. Chinese Journal of Mechanical Engineering, 29, 992-1002. https://doi.org/10.3901/CJME.2016.0519.069

Shi, W., Zhou L., Lu, W., Pei B., Lang, T. (2013). Numerical prediction and performance experiment in a deep-well centrifugal pump with different impeller outlet width, Chinese Journal of Mechanical Engineering, 26 (1), 46-52. https://doi.org/10.3901/CJME.2013.01.046

Shi, Y., Zhu, H., Zhang, J., Zhang, J., Zhao, J. (2018). Experiment and numerical study of a new generation three-stage multiphase pump, J. Petrol. Sci. Eng., 169, 471-484. https://doi.org/10.1016/j.petrol.2018.06.011

Spence, R., Amaral-Teixeira, J. (2008). Investigation into pressure pulsations in a centrifugal pump using numerical methods supported by industrial tests. Computers & Fluids, 37 (6), 690-704. https://doi.org/10.1016/j.compfluid.2007.10.001

Stel, H., Sirino, T., Ponce, F. J., Chiva, S., Morales, R. E.M., (2015). Numerical investigation of the flow in a multistage electric submersible pump. J. Petrol. Sci. Eng., 13, 41-54. https://doi.org/10.1016/j.petrol.2015.10.038

Tao, Y., Yuan, S., Liu, J., Zhang, F., Tao, J., (2017), Influence of blade thickness on transient flow characteristics of centrifugal slurry pump with semi-open impeller. Chinese Journal of Mechanical Engineering, 29, 1209-1217. https://doi.org/10.3901/CJME.2016.0824.098

- Yao, Z. F., Yan, Z. J., Wang, F. J., (2016). Evaluation of near-wall solution approaches for large-eddy simulations of flow in a centrifugal pump impeller. Engineering Applications of Computational Fluid Mechanics, 10 (1), 452-465. https://doi.org/10.1080/19942060.2016.1189362

Yuanyi, L., Yongyan, L., Ruiguang, L. (2009). The Effect of the Clearance Value of Impeller and Draft-tube for the Performance of Stamping Multistage Centrifugal Pumps. In Computer and Communications Security, ICCCS'09. International Conference on pp. 142-145. IEEE.

Zhou, L., Bai, L., Shi, W., Li, W., Wang, C., Y, D. (2018). Numerical analysis and performance experiment of electric submersible pump with different diffuser vanes number. Journal of the Brazilian Society of Mechanical Sciences and Engineering, 40 (2), 89. https://doi.org/10.1007/s40430-018-0986-y

Zhou, L., Shi, W., Lu, W. (2012). Numerical investigations and performance experiments of a deep-well centrifugal pump with different diffusers. Journal of Fluids Engineering, 134 (7), 071102. https://doi.org/10.1115/1.4006676

Zhu, X., Li, G., Jiang, W., Fu, L. (2016). Experimental and numerical investigation on application of half vane diffusers for centrifugal pump. International Communications in Heat and Mass Transfer, 79. 114-127. https://doi.org/10.1016/j.icheatmasstransfer.2016.10.015

Zhu, J., Banjar, H., Xia, Z., Zhang, HQ. (2016). CFD simulation and experimental study of oil viscosity effect on multi-stage electrical submersible pump (ESP) performance. J. Petrol. Sci. Eng., 146, 735-754. https://doi.org/10.1016/j.petrol.2016.07.033